Geophys. J. Int. (2007) **170,** 896–912 doi: 10.1111/j.1365-246X.2007.03408.x

Time-dependent thermal state of the lithosphere in the foreland of the Eastern Carpathians bend. Insights from new geothermal measurements and modelling results

C. Demetrescu,[1,★] H. Wilhelm,[2] M. Tumanian,[1] S.B. Nielsen,[3] A. Damian,[1] V. Dobrică[1] and M. Ene[1]

[1] *Institute of Geodynamics,* 19-21 *J. L. Calderon St., Bucharest, Romania. E-mail: crisan@geodin.ro*
[2] *Geophysical Institute, Karlsruhe University, Hertzstr.* 16*, Karlsruhe, Germany*
[3] *Department of Earth Science, Aarhus University, Høegh-Guldbergsgade* 2, DK-8000*, Aarhus C, Denmark*

Accepted 2007 February 15. Received 2007 February 15; in original form 2005 September 6

SUMMARY

The time-dependent heat budget, thermal evolution and rheology of the lithosphere in the last 13Myr, along a 120 km long profile in the foreland of the Eastern Carpathians bend is presented. The study area, a complex tectonic environment in the vicinity of the well-known intermediate-depth seismogenic Vrancea zone, includes the deepest sedimentary basin in Romania (∼18 km), with a recent rapid evolution in the last 13Myr (8 km of sediments). Detailed high-resolution temperature logs in the depth ranges from 0–700 m to 0–2400 m in eight thermally stabilized boreholes, together with logging and geological information on structure, lithology and time evolution of the sedimentary pile have been used to model the thermal evolution by means of a 2-D finite element model which includes sedimentation history, sediment compaction, lateral and vertical variation of thermal properties of sediments and consolidated crust. Modelling results have been compared to measured temperatures, corrected for palaeoclimate effects, in a trial and error iterative approach.

Sedimentation, palaeoclimate, undercompaction and heat refraction effects on one hand, and the heat generated in the upper crust, on the other, combine to explain the observed subsurface temperature field and in particular the pronounced curvature of the vertical temperature profiles.

The Neogene-Quaternary sedimentation resulted in a rather uniform deficit of the surface heat flux of about 12 mW m^{-2} in the study area, in spite of the marked lateral variation of the sedimentary pile thickness. The palaeoclimate effect is responsible for a surface heat flux depression of 7–8 mW m^{-2}, uniform along the study profile. Unlike older sedimentary basins, in the study area transient sedimentation thermal effects add to palaeoclimate effects in establishing the temperature field in the depth range of geothermal measurements. The lateral variation of the palaeoclimatically corrected surface heat flux from the centre of the Focsani Depression (40 mW m^{-2}) to its margin and the foreland platform (70 mW m^{-2}) is mainly the result of the lateral variation of the heat produced in the upper crust where thickness varies from 7 to 21 km, respectively. A heat production of 2.3 μW m^{-3} for the southeastern end of the profile and of 2.15 μW m^{-3} for the rest of it has been modelled.

As a result of the sedimentation process, temperature variations as large as 70–100°C occurred in the pre-Neogene sediments and the crystalline crust immediately under the sedimentary pile, with consequences on the metamorphic state and rheological behaviour of the foreland

★Now at: Institute of Geodynamics, 19-21 J.L. Calderon st., Sector 2, Bucharest, Romania.

© 2007 The Authors
Journal compilation © 2007 RAS

lithosphere. Progressively smaller variations were present to 40–50 km depth. Unlike flexural modelling, which indicate effective elastic thickness values of 10–15 km, our rheological analysis based on the derived temperature field indicates time-dependent lateral variations between 26–39 km, possibly favouring the recent evolution of the foredeep, characterized by depo-centre migration and basin expansion.

Key words: Carpathians foreland, geothermics, heat flow, lithosphere rheology, sedimentation, thermal modelling.

1 INTRODUCTION

The foreland of the Eastern Carpathians bend (Fig. 1) is composed of several tectonic units separated by crustal-scale faults: the Moesian Platform with the Valachian (Precambrian basement) and the Southern and Central Dobrudjan (Cadomian) sectors, the North Dobrudjan Orogen, the Scythian Platform and the East European Platform. Superimposed on these units is a foredeep (Săndulescu 1984), the external flank of which shows a maximum development in the Focşani Depression. Here, the basement depth reaches 18–20 km (Polonic 1996; Răileanu 1998), making it the deepest sedimentary depression in Romania. The foredeep developed rapidly from the Sarmatian till the present, with ∼8 km of sedimentation in its central parts during the last 13 Ma (Săndulescu 1984; Tărăpoancă *et al.* 2003). It is of crucial importance to understand various consequences of the tectonic evolution of the area, especially in connection to the presence of the adjacent Vrancea seismic zone, the well-known locus of an important intermediate-depth seismicity, and in connection to the strong differential vertical movements that characterize the orogen-foreland system, both at million-years timescale (uplift and erosion in the orogen (Sanders *et al.* 1999), subsidence and sedimentation in the foreland) and at present (uplift in the orogen, subsidence in the foreland (Zugrăvescu *et al.* 1998)). In particular, information on the thermal state of the lithosphere, with important repercussions on its rheological behaviour, obtained by measurements and modelling, would be of great value. Also, the time evolution of the thermal regime of the sedimentary fill in the area could bring insights regarding the hydrocarbon generation process (timing and generated quantities) in such a deep and rapidly evolving sedimentary basin.

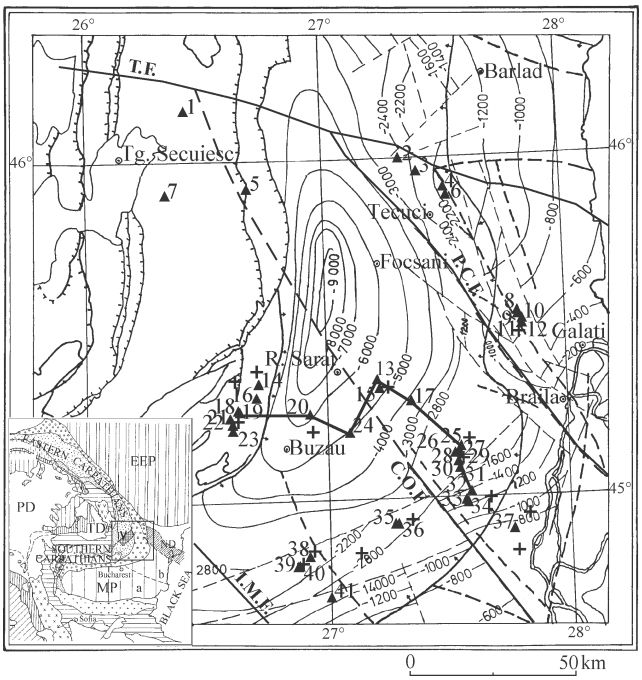


Figure 1. Borehole location in the study area. Tectonics after Dumitrescu & Săndulescu (1970).Triangles—HRT measurements (Demetrescu *et al.* 2005); crosses—temperature measurements with discrete logging (Ene *et al.* 1989–1990); thick line—study profile; labelled isolines—isobaths in meters at the base of Neogene–Quaternary formations; 1–41 identification numbers (Table 1). TF—Trotus fault; PCF —Peceneaga–Camena fault; COF—Capidava-Ovidiu fault; IMF—Intra-Moesian fault. Inset: the study area (rectangle) in the general frame of the Carpathian system; MP— Moesian Platform (a—the Valachian sector, b—the South and Central Dobrudjan sectors), EEP—East European Platform, ND—the North Dobrudjan orogen, V-– epicentral area of intermediate-depth seismicity of Vrncea zone, TD—Transylvanian Depression, PD—Pannonian Depression.

The surface heat flux map of Romania (contours by Demetrescu & Andreescu (1994) after heat flux values of Demetrescu *et al.* (1991/1992) and average regional geothermal gradients obtained using bottom hole temperature data in the foredeep) shows very low values of about 20–30 mW m^{-2}, in the Eastern Carpathians bend foredeep. Temperature measurements by Ene *et al.* (1989–1990) in 14 thermally stabilized boreholes by means of discrete logging with a thermistor probe added to the previous information on the thermal regime of the foredeep, but the maximum investigated depths were only of 500–700 m.

Within the frame of a joint cooperation between the Institute of Geodynamics (Bucharest) and the Geophysical Institute (Karlsruhe University) on heat flow and lithosphere evolution in the East Carpathians bending area and its foreland in four field campaigns in 1997–1999 high resolution temperature (HRT) continuous logs were performed in 41 thermally stabilized boreholes in the area of interest (Fig. 1). The investigated depth range of measurements was significantly larger than previously available, namely eight boreholes were investigated to maximum depths of 700–1000 m, 11 boreholes to 1000–1500 m, and five boreholes to 1900–2400 m. This data set was analysed in a previous study (Demetrescu *et al.* 2005), which concluded that thermal conduction is the primary mechanism of heat transfer in the foreland of the Eastern Carpathian bend. The occurrence of basin-scale fluid flow is not supported by thermal and/or independent evidence. However, first-order calculations showed that the present subsurface temperature distribution most likely is influenced by two transient processes: (1) the recent (13–0 Ma) rapid sedimentation and (2) the palaeoclimate changes of the surface temperature. Furthermore, the occurrence of thick layers of undercompacted shales of low thermal conductivity may be important.

In this paper, we present a transient 2-D analysis of the heat flux budget during the Sarmatian to the present (13–0 Ma) time period along a 120 km long profile across the foreland from the Carpathian nappes through the southern-central part of the Focşani Depression to its margin and Moesian Platform (location in Fig. 1). The

© 2007 The Authors, *GJI*, **170,** 896–912
Journal compilation © 2007 RAS

Table 1. Location and surface heat flux data for the investigated boreholes.

No	No. on map	Borehole	Geographic coordinates Φ Degree	Φ Min	λ Degree	λ Min	Elevation	Investigated depth range (m)	Average gradient (mK m^{-1})	Average conductivity (Wm^{-1} K^{-1})	Surface heat flux Climate corrected (mW m^{-2})
1	19	78 Barbuncesti	45	15.9	26	38.1	303	100–1500	24.6	1.46	43
2	20	303 Bobocu	45	15.8	26	55.9	137	100–2400	23.2	1.58	41
3	24	403 Rosioru	45	12.8	27	5.5	74	100–750	17.2	1.82	46
4	13	103 Boldu	45	21.9	27	12.7	55	100–2100	23.7	1.99	52
5	17	105 Balta Alba	45	18.6	27	21.5	40	100–657	21.8	1.82	52
6	25	309 Oprisenesti	45	10.4	27	33.4	25	100–1402	35.1	1.67	68
7	30	I39 Bordei Verde	45	6.8	27	33.0	24	100–1400	39.7	1.59	70
8	32	817 Liscoteanca	45	2.5	27	35.8	24	100–989	49.9	1.23	69

analysis is based on thermal and lithological data from eight boreholes (Table 1) located on the profile.

The present analysis is a necessary step forward in the attempt to improve the degree of confidence in the obtained results. Rather than comparing determined and calculated surface heat flux values (as is common practice in geothermal modelling), we compare model predictions directly to measured borehole temperatures that have been corrected for the palaeoclimatic influence. As in this case, the transient thermal effects of sedimentation and palaeoclimatic surface temperature changes are mixed together and in principle inseparable, it seems most reasonable first to correct the measured temperatures for palaeoclimate and then model the sedimentation effects and the heat flux budget against the corrected temperatures. In favour of this choice was also the fact that the thermal properties of rocks in the depth interval affected by palaeoclimate effects (down to ∼2 km) are laterally more uniform than those at depths influenced by sedimentation (the entire sedimentary section and the crystalline crust).

In the successive sections of the paper we discuss the principles of the thermal modelling, the temperature data, the information on structure and lithology, the palaeoclimatic correction to the measured borehole temperatures, the resulting temperature field of the lithosphere and the evolution of its thermal state. Furthermore, we discuss the possible rheological consequences for the orogen-foreland system based on the insights gained from the thermal analysis.

2 THE THERMAL MODELLING

The thermal modelling was based on a 2-D finite element model which incorporates changing rates of sedimentation, lateral and vertical variations of the thermal properties of the sediments, sediment compaction, as well as lateral variation of the crustal heat production and of the mantle heat flux. The computer code has been developed within the frame of a cooperation between the Institute of Geodynamics, Bucharest, and the Geophysical Laboratory of Aarhus University (Andreescu *et al.* 2002). A back stripping algorithm (e.g. Steckler & Watts 1978; Sclater & Christie 1980) was used to find the initial thickness of successive sedimentary formations (decompaction) and to evaluate the sedimentation rate. It is assumed that the compaction of sediments is only due to the loss of interstitial water, the time-dependence of porosity being controlled only by the burial depth, z, according to the exponential compaction law $\Phi = \Phi_0 \exp(-z/L)$, where Φ and Φ_0 denote porosities at depths z and, respectively, surface, and L denotes the compaction specific length.

The transient subsurface temperature field is governed by the heat transfer equation:

$$\rho c\left(\frac{\partial T}{\partial t}\right) = \nabla \cdot (\lambda \nabla T) - \rho c \mathbf{u} \cdot \nabla T + H, \quad (1)$$

where T, λ, c, ρ, t, H and $\mathbf{u}$ are the temperature, the thermal conductivity, the specific heat, the density, the time, the heat generation rate and the sedimentation rate, respectively.

The thermal model of the cross-section extends down to 100 km, which is a compromise between the necessity to include all lithospheric heat sources and the need to keep a reasonable proportion between the profile length and the model depth. The conditions at the model boundaries are: constant surface temperature (12°C), constant heat flux at the base and no heat transfer across the vertical boundaries. The mirror effects following from this boundary condition were assessed to be negligible by running the model with extended lengths of the profile. The bottom heat flux of the model is kept constant during the deposition of sediments; its value may be uniform along the entire profile length, or may vary laterally, reflecting thermal effects of possible tectonic processes affecting parts of the lithosphere along the profile.

The solution domain was divided into quadrilateral and triangular elements, according to the lithospheric structure before the sedimentation. The nodal density of the finite element grid was designed to decrease toward the surface in order to achieve a finer resolution in the crust and sediment. The Galerkin finite element approximation was used to transform the differential heat eq. (1) into a matrix form Akin (1984). Details about the representation of sedimentation and erosion are given in Appendix A and in Andreescu *et al.* (2002).

3 OBSERVATIONS

3.1 Temperature data

Temperature measurements were recorded by means of a logging tool provided by the Geophysical Institute. It consists of a PT100 sensor at the tip of a temperature probe mounted on a 3000 m single conductor armoured cable connected on a winch with a depth counter and a recording system. The tool has a resolution of 1 mK and measures the temperature at a sampling rate of 1 or 2 s on demand. It is calibrated in a heat bath using a Hewlett-Packard Quartz thermometer 2804A with an accuracy of 0.02°C in the temperature

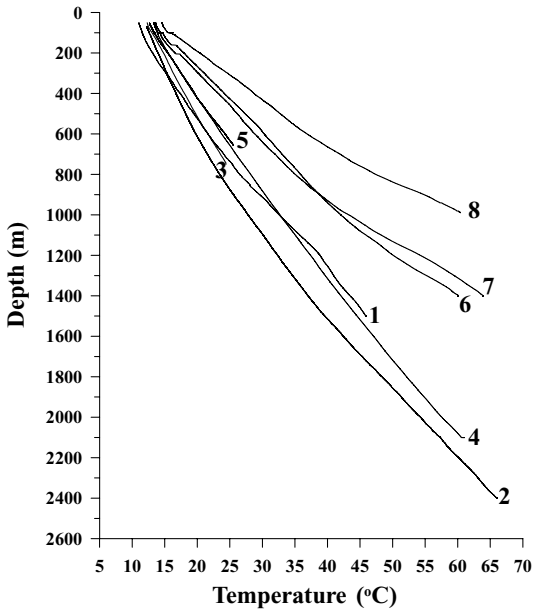


Figure 2. Temperature logs of the eight boreholes on the profile. 1–8-– identification numbers (see Table 1 for correspondence with map numbers).

range 5–95°C. Its ambient stability is 0.03°C in the temperature range 0–55 °C. All boreholes were in a steady-state thermal regime achieved after a long period of rest (years) after the shut down. The logged temperatures in the eight boreholes retained for this study are presented in Fig. 2. Temperature logging began after an appropriate rest-time of the sensor at depths of 50–60 m, necessary to accommodate the temperature probe from summer surface temperatures (25–35°C) to borehole temperatures (10–15°C).

The temperature logs were processed to obtain the geothermal gradient. Taking into account the precision of temperature measurements (±0.005 K), a minimum depth interval to get a thermal gradient within ±1 mK m^{-1} would be 10 m. Depth intervals of 10 m will ensure a gradient value within 5% of its true value, in case of a gradient of 20 mK m^{-1}, and within 2.5%, in case of a gradient of 40 mK m^{-1}. The thermal gradient was computed from moving pairs of temperature data points separated by approximately 10 m (the actual depth interval is controlled by the sampling rate and velocity of the thermometer), and these values were assigned to the middle of the corresponding depth interval. In Fig. 3, the variation of the geothermal gradient along profile in the depth range of temperature measurements is presented.

A large range of lateral variations of the vertical temperature gradients characterizes the temperature field in the study area (Figs. 2 and 3). The gradient values range from 18 mK m^{-1} in the area of maximum thickness of the foredeep to 35 mK m^{-1} and 50 mK m^{-1} at its margins and on the Moesian Platform. Also apparent is an increase of the geothermal gradient with depth. It is a primary criterium of success of our transient 2-D analysis that these first-order features are reproduced.

3.2 Lithosphere structure along profile. Sedimentation history

The general structure of the sedimentary pile in the Carpathians bend foredeep is well known. To constrain the structure along profile, in the present study we used information from published geological maps (Romanian Geological Survey, 1968) from borehole data available at oil companies, and from literature (Dumitrescu & Săndulescu 1970; Paraschiv 1979; Săndulescu 1984; Damian 1996). A recent discussion of the architecture of the Focşani Depression is presented by Tărăpoancă *et al.* (2003), based on a large database consisting of 2-D seismic lines and borehole data. In Fig. 4 the structure of the Neogene sedimentary pile is shown, together with characteristic moments of the time history of sedimentation. The structure in the upper part of the cross-section is constrained with available electrical logs (self potential and resistivity) for the eight boreholes on the profile. Information from an additional borehole (922 Ghergheasa) located close to the profile is also used.

The Neogene sedimentation began in the foreland in the Badenian (16.2 Ma). The Focşani Depression is characterized by rapid accumulation of ∼8 km of sediments in the area of maximum

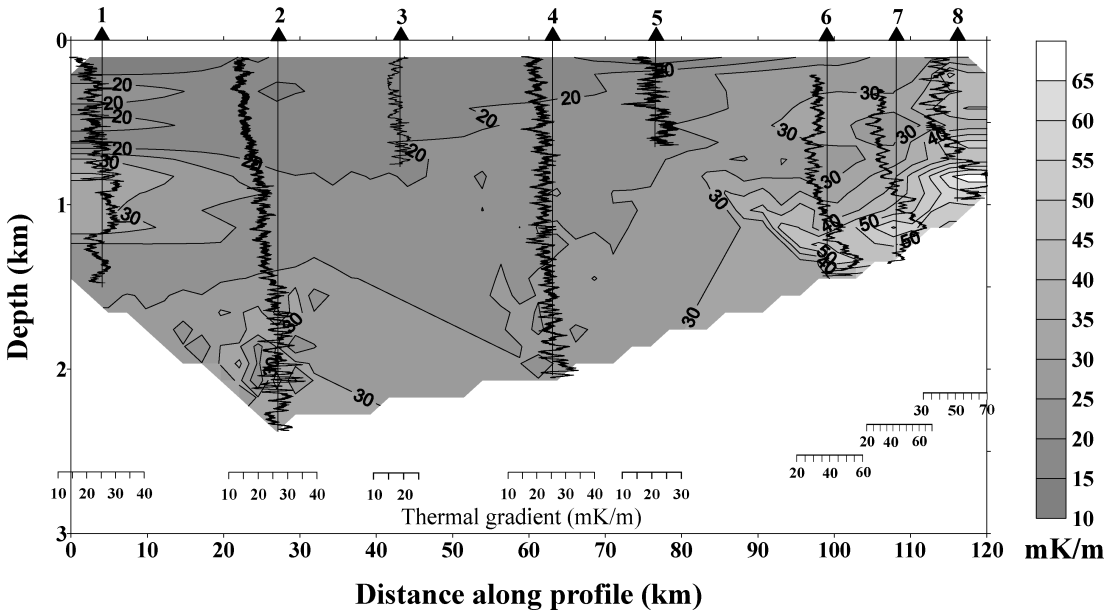


Figure 3. The lateral distribution of the geothermal gradient as determined from temperature measurements. Contours in mK m^{-1}. The vertical profiles of the geothermal gradient (TG) are superimposed. Note the different TG scale for the boreholes no. 6, 7, 8. Triangle—borehole.

© 2007 The Authors, *GJI*, **170,** 896–912
Journal compilation © 2007 RAS

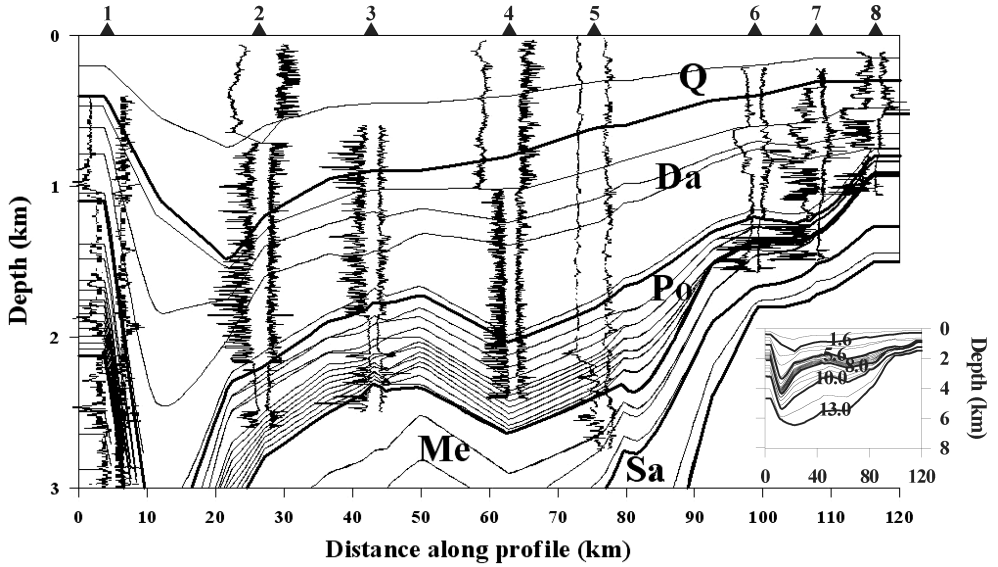


Figure 4. Structure of the upper part of the sedimentary pile along the study profile as constrained by borehole data (electrical logs and general information). Q—Quaternary, Da—Dacian, Po—Pontian, Me—Moetian, Sa— Sarmatian. Inset: starting time for the deposition of the five sedimentary formations (Myr before present). Thin lines: subdivisions with different thermal properties.

thickness (∼6 km on the profile) from the Sarmatian to the Present (13–0 Ma) (Fig. 15). In the southern part of the basin, the Badenian sediments (16.2–13.0 Ma) are much thinner than in the central part and along our profile they are missing. The Upper-Miocene deposits, especially those of Pontian age (7.0–5.4 Ma), are primarily made of shales, which were encountered in boreholes in the southern part of the depression. A change of the sedimentary facies is noticed in the Dacian (5.4–2.7 Ma) and Pliocene (2.7–1.6 Ma) (mixture of shales and sands, in which shales dominate in Dacian deposits). In the Pleistocene (1.62–0.01 Ma), the sedimentation regime changes again by the appearance of gravel deposits (Bădescu 1998).

Figure 5 shows crustal-scale structures of the model obtained from maps published by Polonic (1996) (basement) and Rădulescu (1988) (the Conrad and the Moho discontinuities).

The lithosphere thickness in the study area was estimated at ∼180 km by Demetrescu *et al.* (1984) and Rădulescu *et al.* (1985), using 1-D geothermal modelling, and by Stănică and Stănică (1984), using magneto-telluric sounding. A value of 70–80 km was obtained by Enescu (1992), based on the depth of reflection point for certain waves identified on seismograms. Besides the different definitions of the lithosphere/asthenosphere boundary implied in the various methods used to evaluate the lithospheric thickness, it seems that in this case the seismological method is not sensitive enough, as the velocity contrast between the lithosphere and the asthenosphere was small.

3.3 Material properties. The thermal conductivity model

Modelling of the subsurface temperature field requires knowledge of the physical properties of sediments and basement rocks. However, core sampling by the oil companies has focused on the reservoir sections well below our logging depths wherefore no samples were available for laboratory measurements of thermal conductivity and other petrophysical properties. Also, only electric logs are routinely

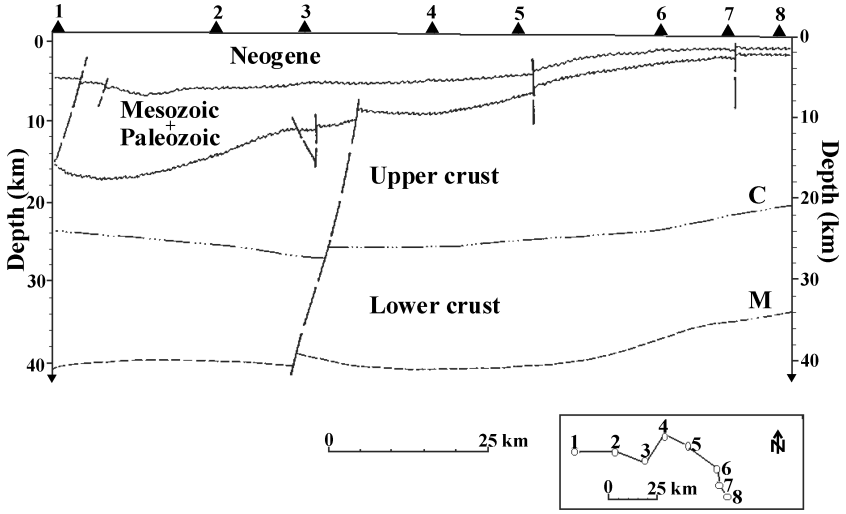


Figure 5. Crustal cross-section along the study profile. Triangle—borehole. Inset: actual form and orientation of the study profile. C —Conrad discontinuity; M—Mohorovičić discontinuity.

© 2007 The Authors, *GJI*, **170,** 896–912
Journal compilation © 2007 RAS

run which prevented us to apply methods devised to assess thermal conductivity from well logs (Demongodin *et al.* 1991; Vasseur *et al.* 1995).

Generally, in a 1-D steady-state conductive regime with no heat production, the temperature gradient log would be a proxy for the depth-dependence of the thermal conductivity (Blackwell & Steele 1986). If one sector of the borehole could be calibrated as regards the thermal conductivity of rocks, an 'absolute' depth-dependence of this parameter would be obtained by comparing thermal gradient values in various sections of the borehole. If not, only a relative depth-variation of the conductivity is obtainable. However, the transient thermal effects of palaeoclimate variations of the surface temperature and of sedimentation make it impossible directly to use the geothermal gradient for this purpose, unless such effects are assessed and the steady-state temperature field is recovered from measured temperature data.

In this study, estimations of thermal conductivity and other physical properties were obtained from the average lithology derived from stratigraphic columns of published geological maps (Romanian Geological Survey, 1968), from borehole information available at oil companies, and/or from the literature (Paraschiv 1979). For the upper part of the cross-section the lithology has been derived by interpreting electric logs in terms of rock composition. In Fig. 4 electric logs have been superimposed on the adopted structure of the sedimentary pile, to illustrate this approach. The lithological model of the cross-section and the corresponding thermal conductivity model, used in the first iteration of the trial and error procedure adopted to reduce the difference between the modelled and the measured temperatures corrected for palaeoclimate are shown in a simplified form in Fig. 6 and Fig. 7, respectively. In the next iterations, the thermal properties of the sedimentary formations are locally changed in order to achieve a better fit of calculated temperatures to the measured ones, corrected for palaeoclimate.

For rock mixtures, thermal conductivity was derived by a geometric mean formula (e.g. Beck 1976), knowing the properties of components and their volume fraction:

$$\lambda = \prod_i (\lambda_i)^{V_i}, \tag{2}$$

where λ_i is the thermal conductivity and V_i is the volume fraction for rock of type i. The same formula is used in case of porous rocks, with two components – the solid matrix and water. The case with oil (thermal conductivity 0.15 $\mathrm{Wm^{-1}\ K^{-1}}$) instead of water (0.6 $\mathrm{W\,m^{-1}\ K^{-1}}$) is only local and implies small volumes, not 'seen' in a 2-D simulation at the scale considered. For each rock type, the porosity is decreasing with depth according to $\Phi_i = \Phi_{oi} \exp(-z/L_i)$, where Φ_{oi} is the surface porosity and L_i the compaction constant. Φ_i and L_i are included in eq. (1) via the thermal conductivity, λ_i, and the sedimentation rate, **u**. Weighted means were used for the other parameters (density, heat generation rate). The mixing law for the heat capacity is $\overline{\rho c} = \sum_i \rho_i c_i V_i$, with $\rho = \sum_i \rho_i V_i$. The thermal conductivity, thermal diffusivity, density, radiogenic heat production, compaction constant and surface porosity for each rock type from the stratigraphic column were evaluated from literature

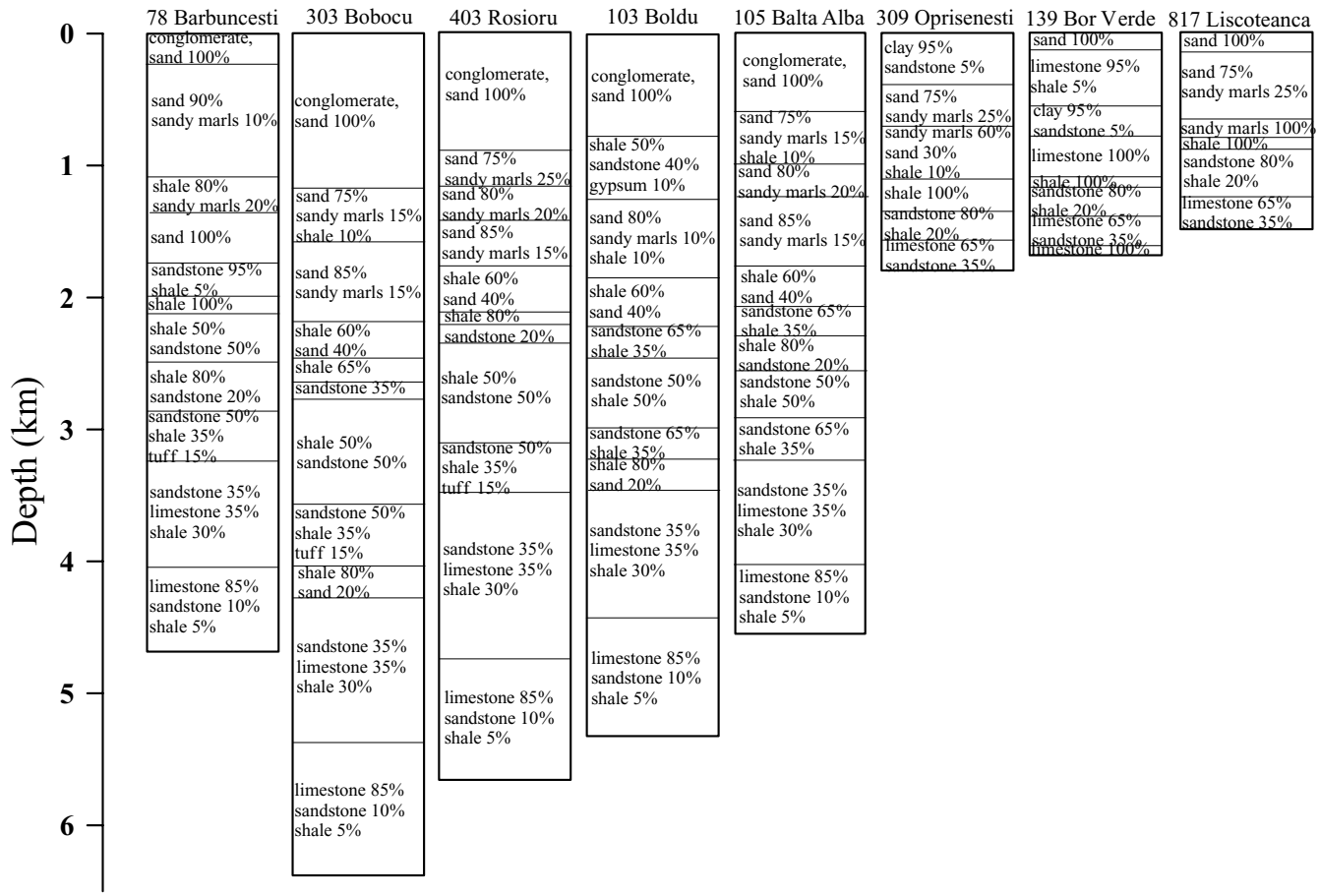


Figure 6. Simplified composition of the sedimentary pile at boreholes.

© 2007 The Authors, *GJI*, **170,** 896–912
Journal compilation © 2007 RAS

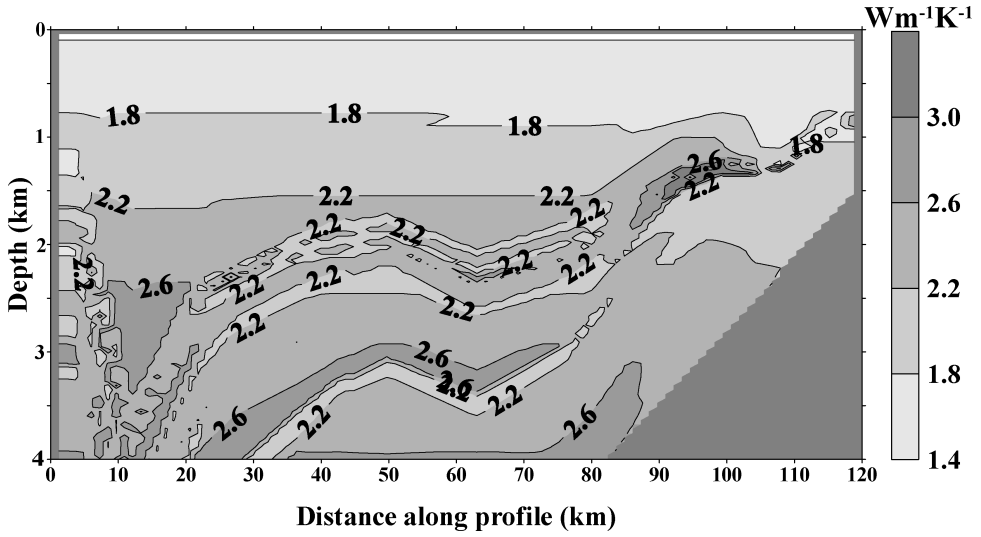


Figure 7. Upper part of the starting thermal conductivity model along profile.

Table 2. Material properties of the lithologic model of sediments (Kappelmeyer & Haenel 1974; Hutchison 1985; Issler & Beaumont 1986).

Sediment type	ρ (kg m^{-3})	Φ_o (%)	L (km)	λ (W m^{-1} K^{-1})	c (W s kg^{-1} K^{-1})	A (μW m^{-3})
SAND	2650	60	2.8	4.5	800	0.2
LOESS	1600	70	2.0	1.0	850	1.0
LIMESTONE	2710	70	1.5	3.0	850	0.1
SANDSTONE	2650	62	2.78	4.2	1088	0.84
CLAY	2600	70	2.0	1.0	850	1.0
SHALES	2700	48	0.61	1.7	748	1.3
CONGLOMERATE	2650	60	2.0	2.5	850	0.2

information (Kappelmeyer & Haenel 1974; Hutchison 1985; Blackwell & Steele 1986; Issler & Beaumont 1986; Magara 1986; Schön 1996). Values most used in modelling temperature field of lithosphere (Beck & Shen 1989; Čermák *et al*. 1989; Čermák & Bodri 1991; Čermák 1995) were adopted for the thermal properties of crustal and subcrustal lithosphere rocks. The values of the material parameters used in our modelling are given in Table 2 for sediments and in Table 3 for the crust and the subcrustal lithosphere. In case of lower crust thermal conductivity, a value of $\sim$2 Wm^{-1} K^{-1}, corresponding to a mafic composition is generally preferred (e.g. Čermák *et al.* 1989). However, the composition of the lower crust is less constrained than of other lithospheric layers being mainly controlled by observation on seismic velocity (Holbrook *et al.* 1992; Afonso & Ranalli 2004). In case of our study area, values in the range 6.7–7 km s^{-1} have been determined (Hauser *et al.* 2001), corresponding to a mixture of intermediate and mafic rocks, characterized by an increased thermal conductivity (3.1 Wm^{-1}K^{-1}, Schön 1996). This choice does not change the temperature field derived for the upper crust and sedimentary layers, but would produce smaller temperatures by 50–60 °C in the lithospheric upper mantle and a thicker by about 10 km thermally defined lithosphere.

As regards the porosity–depth relationship, there are differences in the behaviour of shales as compared to other rocks. While sandstones exhibit a relatively constant porosity reduction with depth, shales show some peculiarities. Magara (1986), in a study with data from many sedimentary basins showed that at shallow depths, porosity decreasing with depth is rapid, in contrast with what happens at larger depths. The same study also indicates the existence of deep zones in which the shale porosity is abnormally high (undercompacted shales). Analysing sonic, electric and neutron logs, as well as seismic, regional geology and geothermal data Damian (1996) inferred the existence of undercompacted shale deposits of thicknesses up to 400 m in the Focşani Depression. In such undercompacted sediments with relatively low thermal conductivity, the geothermal gradient is larger than in a normally compacted depth interval, for pure conductive heat transfer. In our thermal model, the undercompaction is simulated by adopting a much larger compaction constant L than the one given in Table 2, indicated by Issler & Beaumont (1986).

4 PALAEOCLIMATE CORRECTION

It has been shown by Demetrescu *et al.* (2005) that palaeoclimate changes of the surface temperatures are likely to produce significant effects on subsurface temperatures down to $\sim$2500 m in the study area and consequently on the surface heat flux inferred from measured data.

Table 3. Thermal properties of the mantle and the crust (Beck & Shen 1989; Čermák *et al.* 1989; Čermák & Bodri 1991; Čermák 1995).

	λ (Wm^{-1} K^{-1})	A (μW m^{-3})	ρ (kg m^{-3})	c (W s kg^{-1} K^{-1})
UPPER CRUST	3.1	1.1	2700	900
LOWER CRUST	3.1	0.1	2900	900
MANTLE	4.0	0.0	3300	1000

© 2007 The Authors, *GJI*, **170,** 896–912
Journal compilation © 2007 RAS

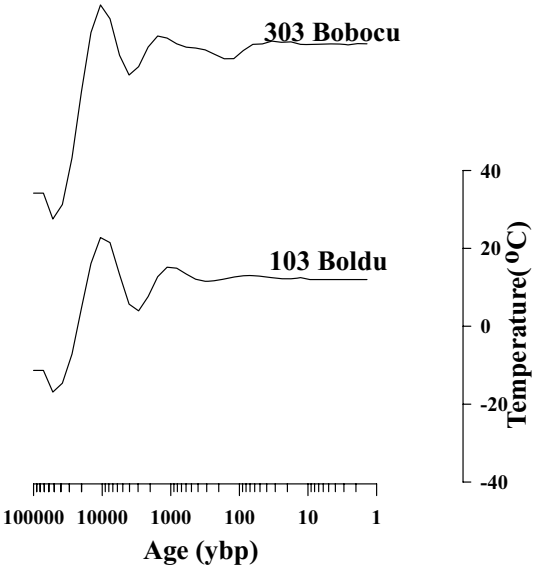


Figure 8. GSTH in case of the two deepest investigated boreholes from inversion of the measured temperatures.

Inversion methods applied to measured temperatures yield unreasonable large variations of the ground surface temperature history (GSTH), as shown in Fig. 8. This happens because measured temperatures also contain information on the sedimentation, its transient thermal effects being mapped by the inversion procedure in the resulting GSTH. The inversion has been based on the least squares formulation of Tarantola & Valette (1982a, 1982b). Details on the inversion procedure have been presented by Şerban *et al.* (2001b).

The forward modelling in this case is the only solution to account for palaeoclimatic changes in the study area. Calculations have been made for the GSTH model published by Beck (1977). Results are presented in Fig. 9. The left panel shows the temperature variations induced by the GSTH and the right panel shows the corrections to be applied to the measured thermal gradient.

The plots show similar behaviour at all eight studied boreholes of both temperature disturbance and thermal gradient disturbance produced by the given GSTH. The temperature disturbance has a maximum value of $\sim -4^{\circ}$C at 1000 m depth and values of -1 to -2°C at shallower (100–300 m) and deeper (>2400 m) levels. The palaeoclimate correction to the geothermal gradient would be of ~ -1 to -3 mK m^{-1} at depths larger than 1200 m and of between $+6$ and -2 mK m^{-1} depending on depth in the depth interval 400–1200 m. Calculations of the palaeoclimatic correction have been done by means of the FEMLAB (Finite Element Method Laboratory) software (©COHSOL AB). The distribution of the corrected thermal gradient along the profile is presented in Fig. 10.

The accuracy of the palaeoclimate correction evidently depends on the input GSTH and to a lesser extent on the thermal properties of the rocks in the depth interval considered. The GSTH model of Beck (1977), widely used, is a result of integrating information on palaeoclimate from proxy data, such as coral reefs, tree rings, palinology, $^{18}O/^{16}O$ ratio variations in ice cores. The model indicates a step increase of temperature of 12 K at the end of the Weichselian glaciation (10000 ybp, see inset Fig. 9). Calculations on synthetic data show (Şerban *et al.* 2001a) that every single degree increase in the amplitude of temperature variation related to the last glaciation causes about 1 mW m^{-2} of decrease in surface heat flux. Given a thermal conductivity of about 1.8–2.2 W m^{-1} K^{-1} characteristic for rocks in the sampled depth interval (Fig. 14), the effect in the geothermal gradient correction will be an increase of about 0.55–0.45 mK m^{-1}. Şerban *et al.* (2001b) inferred, by inversion of vertical temperature profiles from nine boreholes in the Transylvanian Basin that the glacial temperature drop as compared with the present surface temperature is in the range 3.5–15 K with an average of about 11 K. Other studies (Clauser *et al.* 1997; Šafanda & Rajver 2001; Demezhko & Shchapov 2001; Mareschal *et al.* 1999) show similar values for the glacial/postglacial warming: 10 K at the superdeep borehole KTB-HB, Germany, 6–14 K in case of three Czech boreholes, 7 and 11 K in case of two Slovenian boreholes, 13 K in case of a Ural superdeep borehole, 10 K in case of a Canadian borehole, respectively. A recent review of forty-eight estimates of Pleistocene/Holocene warming

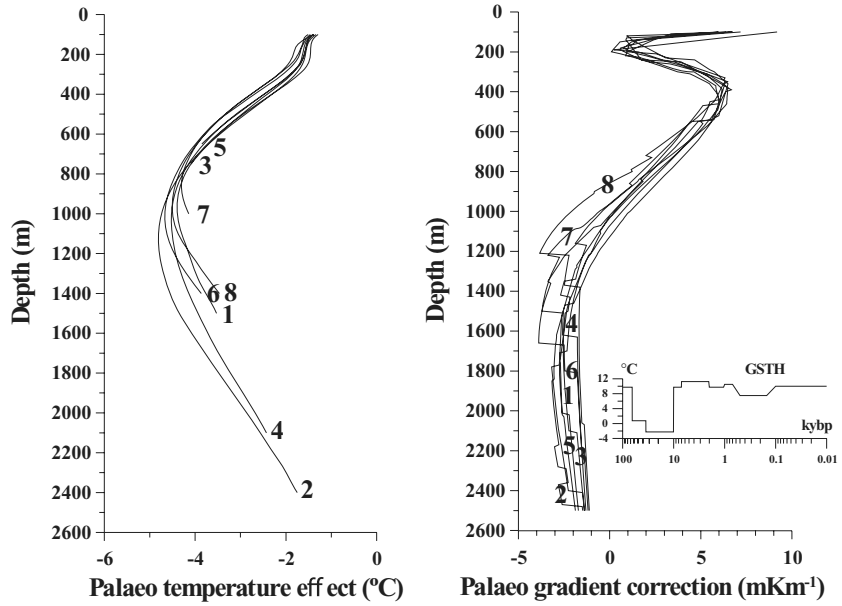


Figure 9. Left: thermal effect of the GSTH of Beck (1977) for the eight boreholes on the study profile. Right: correction for palaeoclimate variations (Beck's (1977) model) applied to the determined geothermal gradients. 1–8–– identification numbers.

© 2007 The Authors, *GJI*, **170,** 896–912
Journal compilation © 2007 RAS

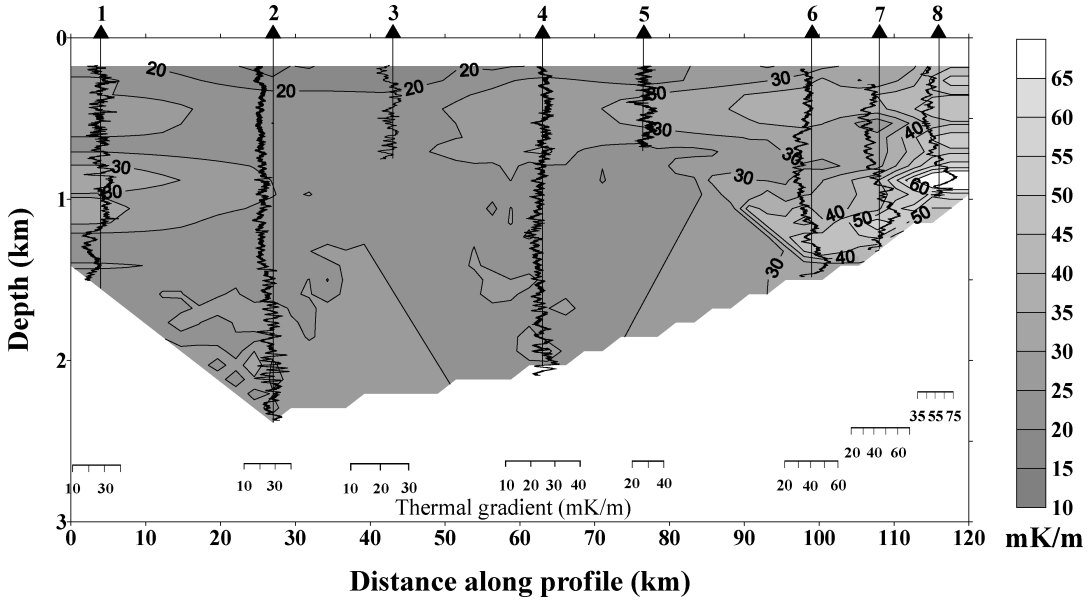


Figure 10. Palaeoclimate corrected geothermal gradient along profile. Contours in mK m^{-1}. The vertical profiles of corrected geothermal gradient are superimposed. Note the different TG scale for the boreholes no. 6, 7, 8.

amplitude in Europe (Demezhko *et al.* 2006) shows values between 8 and 23 K.

In the next section, the thermal modelling by a trial and error approach in which the 2-D finite element modelling results are compared with palaeoclimatically corrected temperatures will give information on the heat flow budget and temperature field of the lithosphere.

5 RESULTS AND DISCUSSION

5.1 The heat flux budget

Generally, the surface thermal field features in a certain area are a result of superposition of the heat contributed from the mantle and crust by tectonic processes involving the entire lithosphere (such as subduction, extension, thickening) and of the thermal effects of shallower processes with local extension, such as sedimentation, radiogenic heat generation in sediments, and fluid flow. An important feature of the thermal field in the foreland of the Eastern Carpathians bend, which should be explained by modelling, is the observed increase of the thermal gradient (and consequently of the surface heat flux) toward the south-eastern end of the study profile. In the following, we shall present the results concerning the contribution of various heat sources to the thermal regime of the study area, as derived in our approach.

As mentioned above, the criterium used in modelling was the fit of the numerically calculated results with the measured temperatures corrected for palaeoclimate changes. In Fig. 11, the residuals (differences between corrected and calculated values) in case of the accepted final model are given, showing a very good fit of within ±1K. In Fig. 12, the fit is detailed for the deepest measured borehole namely 303 Bobocu. The model output (thin line) is fitting the paleoclimate corrected (dash-dot line) temperature. The thick line is the measured temperature and the dashed line is the temperature at thermal equilibrium.

5.1.1 The mantle heat flux

Previous studies (Demetrescu & Andreescu 1994; Andreescu & Demetrescu 2001) have demonstrated how the pre-Neogene subduction in the East Carpathian area could have influenced the thermal regime at large depths, in agreement with the intermediate-depth seismicity of Vrancea area. We interpret the relatively low-mantle heat flux value required by the present sedimentation model as the expression of this earlier finding.

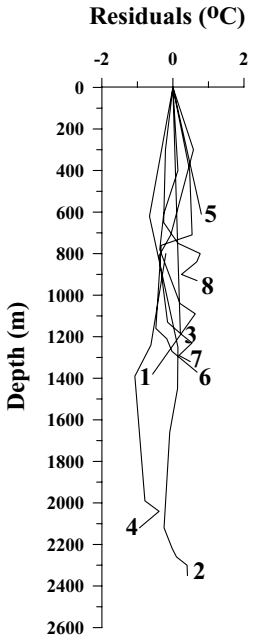


Figure 11. Residuals of fitting temperatures in the sedimentation model to measured temperatures corrected for palaeoclimate.

At the eastern and southeastern basin margins, another tectonic process involving the entire lithosphere is likely to have been acted as an additional heat source, namely the extension in Badenian (16.2–13 Ma) which is at the origin of small-scale basins evidenced by Tărăpoancă *et al.* (2003). Significant non steady state amounts of heat can be stored in such a lithosphere (McKenzie 1978). Demetrescu & Polonic (1989) showed, for instance, that moderate

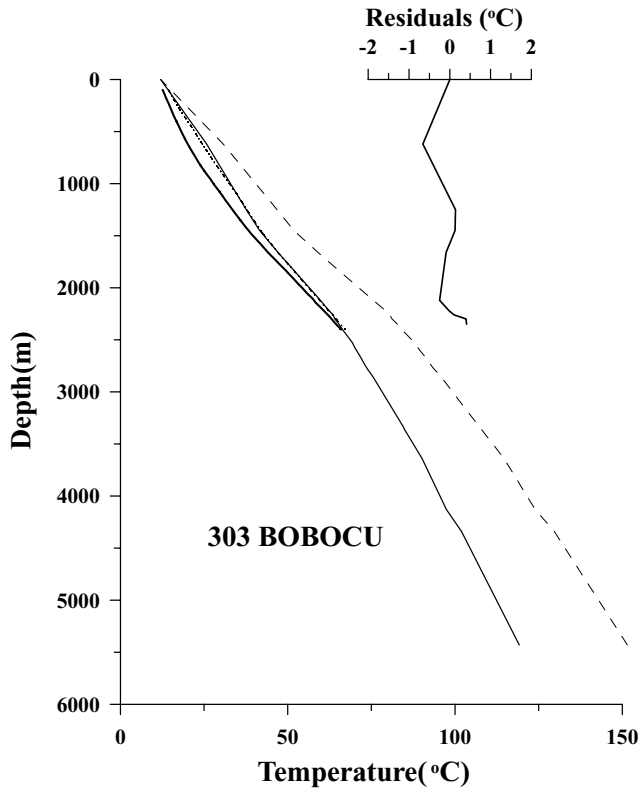


Figure 12. Details of the fit in case of 303 – Bobocu borehole. Thick line—measured temperatures; dash-dot line—palaeoclimate corrected temperatures; thin line—modelled temperatures; dashed line—equilibrium temperature after infinite time. Residuals = palaeoclimate corrected temperatures minus modelled temperatures.

extensions of a few per cents added as much as 15–17 mW m^{-2} to the heat flow budget of the Pannonian Depression, as a consequence of the Badenian extension episode in its history. However, in case of the small basins mentioned, Tărăpoancă *et al.* (2004) showed that the maximum synrift extension was of only 1% and had no thermal consequences on the subsequent evolution of the area. Besides, the alternative option to the uniform mantle heat flow along the profile, namely a laterally varying mantle heat flow (see Section 2 – boundary conditions), with higher values toward the southeastern end of the profile thought to contribute to the higher thermal gradients observed there was shown by our modelling to have only the general effect of a uniform shift of the modelled surface heat flux due to the 2-D nature of the heat transfer to the surface. Only sources closer to the surface, such as the radiogenic heat producing upper crust or basin scale fluid flow could produce the higher surface heat flux observed at the southeastern end of the profile. The former is discussed in the next subsection. The latter has been accepted by Demetrescu *et al.* (2005) in the absence of thermal and/or independent evidence to play no significant role in this respect.

As regards the mantle heat flux, the best fit has been obtained in case of a uniform value of 28 mW m^{-2} along the profile. Such a relatively low-mantle heat flux is compatible with the large thickness of the lithosphere in the study area (Demetrescu *et al.* 1984; Stănică & Stănică 1984) and/or with subduction processes related to the presence of intermediate depth seismicity in the Vrancea area (Demetrescu & Andreescu 1994; Andreescu & Demetrescu 2001).

5.1.2 The crustal heat production

It is well known that an important contribution in the heat flow budget of a certain area comes from the radiogenic heat production in the upper crust (e.g. Rybach 1988). Andreescu (1993) showed that in the Valachian sector of the Moesian Platform, lateral variations of the heat generation rate in the basement might be present, related to intrusive bodies with higher radiogenic heat productivity known in the area (Paraschiv 1979). In the study area, the presence of several crustal blocks (Fig. 1) with different ages and most probably of different types of crust, with different heat production, is most probably the best candidate to explain together with the lateral variations in the sedimentation process, the observed lateral variations in the subsurface temperature field. Lateral variations in the crustal heat production were invoked by Demetrescu *et al.* (1981, 2001) and Andreescu *et al.* (2002), in case of the Transylvanian Basin, and by Pasquale *et al.* (2001), in case of the boundary zone between the Alps and the Apennines to explain the heat flow deficit characterizing the centre of the Transylvanian Basin and, respectively, the heat flow contrast observed in the boundary zone between the Alps and the Apennines.

In the lower panel of Fig. 13, the final model of the crustal heat generation rate is presented. Our modelling required a heat production of 2.3 μW m^{-3} for the crustal block situated at the southeastern end of the study profile and a value of 2.15 μW m^{-3} for the rest of the profile. With these figures, the contribution of the upper crust to the surface heat flux would vary along the study profile from $\sim$15 mW m^{-2} in the deepest part of the basin (7 km of upper crust) to $\sim$36 mW m^{-2} in the central part of the profile (17 km of upper crust) and to about 45 mW m^{-2} in the platform area at the southeastern end of the profile (21 km of upper crust). The contribution

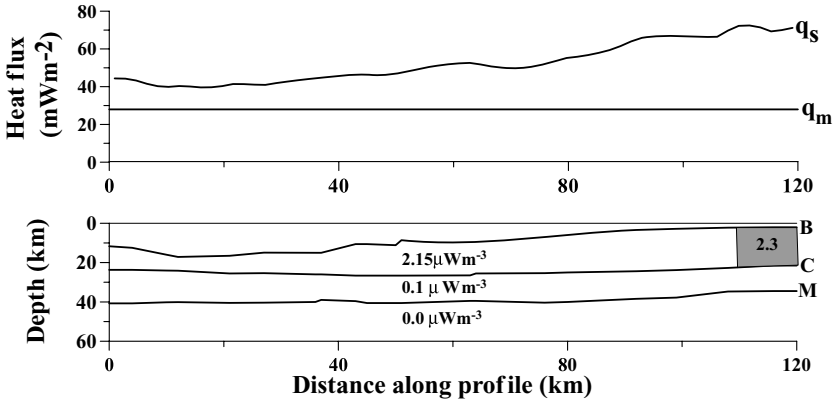


Figure 13. Modelled crustal heat production (lower panel) and modelled surface (q_s) and mantle (q_m) heat flux (upper panel).

© 2007 The Authors, *GJI*, **170,** 896–912
Journal compilation © 2007 RAS

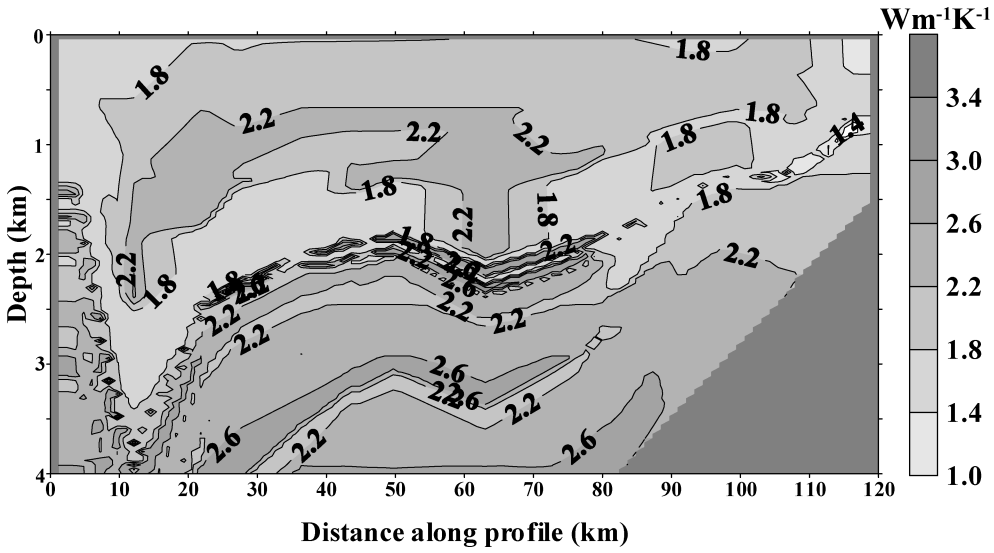


Figure 14. Final model of thermal conductivity for the upper part of the sedimentary pile.

of the heat production of sediments to the heat balance varies along profile, between 3.9 mW m^{-2} in the deepest part of the basin (6 km of Neogene sediments) and 0.9 mW m^{-2} (2 km of Neogene sediments) at the eastern end of the profile. The heat generation rate of the sediments takes values in the range 0.2–1.2 μW m^{-3}, depending on composition, as discussed in Section 3.3.

5.1.3 Thermal conductivity of sediments. The surface heat flux

The final model of thermal conductivity distribution in the upper part of the sedimentary sequence is given in Fig. 14. One can notice layers at depths of 2–3 km, with lower thermal conductivity corresponding to undercompacted formations, between formations with higher conductivities.

Thermal conductivities and temperature gradients from the elements corresponding to the formations deposited in the depth range of temperature measurements are used to calculate the surface heat flux. The results are shown in the upper panel of Fig. 13. The values vary laterally between ∼40 mW m^{-2}, in the deepest part of the depression, to ∼70 mW m^{-2} on the Moesian Platform, at the SE end of the profile. Note that these are surface heat flux values corrected for palaeoclimate. The calculated values for the eight boreholes of the study are given in Table 1, together with the average geothermal gradient and the average thermal conductivity for each borehole. Second-order variations in the lateral distribution of the surface heat flux along profile come from heat refraction effects produced by laterally varying thermal conductivities.

5.2 The time evolution of the temperature field of the crust

The geodynamic processes of basin formation generally involve the redistribution of mass and heat in the lithosphere/astenosphere system (e.g. McKenzie 1978). The resulting temperature history of the sedimentary fill is of primary importance to the understanding of hydrocarbon generation and of rheological properties of the underlying lithosphere and depends on the initial basin forming process. Furthermore, the thermal blanketing effect provides an important thermal feedback on the lithospheric thermal structure. The deposition of sediment produces a general increase in lithospheric temperatures because of the sediment blanketing, and a decrease in the

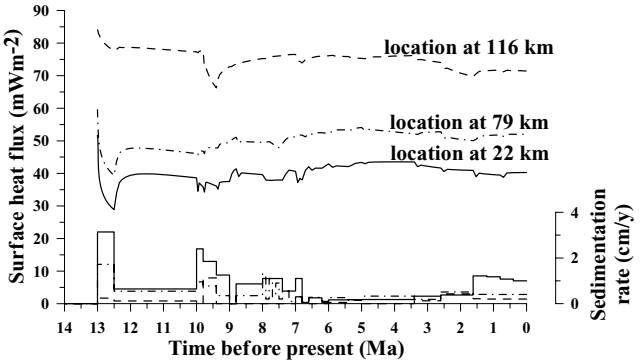


Figure 15. Time-dependent surface heat flux and sedimentation rate at three locations on the study profile.

surface heat flux. The heating of the sediments during and after their deposition consumes heat, contributing in turn to the time-dependent heat balance of the system. Also, the heat production of the deposited sediments contribute the heat budget in the upper part of the upper mantle – lithosphere – sediments system. The variation of the surface heat flux during sedimentation is illustrated in Fig. 15 by the evolution in the last 13 Ma of the surface heat flux at three locations along profile (22, 79, 116 km). The sedimentation rate, as computed from the thicknesses of various deposited formations, that resulted by applying the decompaction procedure mentioned in Section 2, is also shown in Fig. 15. The strong dependence of the surface heat flux evolution on the sedimentation rates is evident. For instance, the Sarmatian sedimentation episode depressed the surface heat flux by as much as 23 mW m^{-2} in the deepest part of the depression (location at 22 km from the western end of the study profile). This figure gradually diminished to 13 mW m^{-2} in the next 1.5 Ma. Much smaller fluctuations, produced by subsequent sedimentation episodes can also be seen. At present, there is a deficit of the surface heat flux as compared to the case of thermal steady state of the basin, of about 12 mW m^{-2}, rather uniform along the study profile. Differences between the deepest part of the Focşani Depression and the southeastern end of the profile appeared only in high sedimentation rate episodes (e.g. Sarmatian). In Fig. 16, the lateral variation of the surface heat flux along profile for specified moments of the basin

© 2007 The Authors, *GJI*, **170,** 896–912
Journal compilation © 2007 RAS

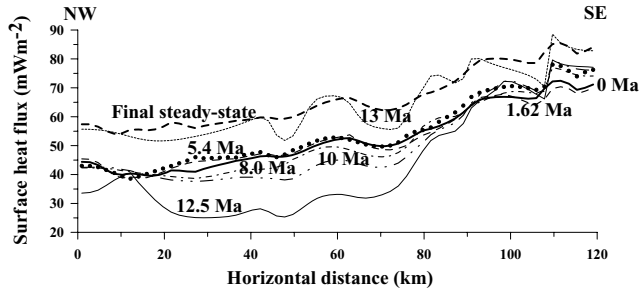


Figure 16. Surface heat flux along the study profile at characteristic moments before present and at the future thermal equilibrium.

history is presented. Again, one can see the pronounced depression of the surface heat flux during the first 0.5 Myr of the Sarmatian and the subsequent recovery on which secondary episodes of depression are superimposed (e.g. the Quaternary sedimentation in the south-eastern end of the profile), depending on the sedimentation history in particular places along the profile. The second-order rather pronounced lateral variations in the initial heat flux profile (13Ma) – a result of heat refraction are gradually smoothed in the successive heat flux profiles as sedimentary layers are added. The lithosphere will reach eventually, if no other tectonic processes will intervene, a thermal steady state with a surface heat flux (thick dashed line in Fig. 16) larger than the initial one by the contribution of the heat production of the sediments.

The heating of the crust below the sedimentary basin is illustrated in Fig. 17, where isotherms show the present day temperature field (continuous lines) and the temperature of the same crustal volumes before the Neogene sedimentation (thin broken lines). The general structure of the crust is superimposed (thick lines). As a result of the sedimentation process, temperature variations as large as 70–100°C (about 80% of the initial temperature) occurred in the crystalline crust immediately under the sedimentary pile. They are progressively smaller to 40–50 km depth. Also, a lateral migration of the transient thermal anomaly induced in the crust by the deposition of Sarmatian sediments is noticed. At present, the maximum of that anomaly is to be found in the central part of the cross-section. Temperature changes experienced by crustal rocks are also illustrated in Fig. 18 by means of the evolution of geotherms (crustal vertical temperature profiles) at the location corresponding to the deepest part of the basin. Rocks at top pre-Sarmatian, basement (B), mid crust (C), lower crust and crust bottom (M) are marked by symbols (cross, star, rhomb, circle and square, respectively). Note

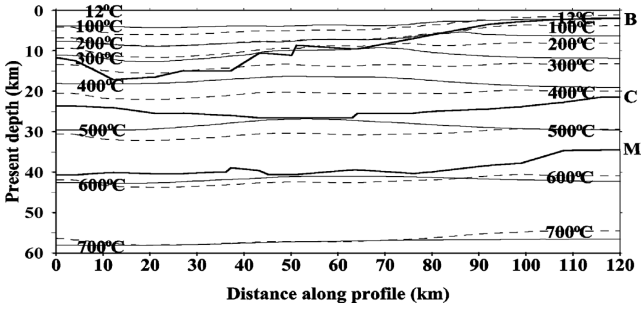


Figure 17. Modelled present temperature field along the study profile (thin lines, left-hand labels) and the temperature of the same rock volumes before the Neogene–quaternary sedimentation (broken lines, right-hand labels). Present crustal structure is superimposed (thick lines) B—crystalline basement, C – Conrad discontinuity, M—Mohorovičić discontinuity.

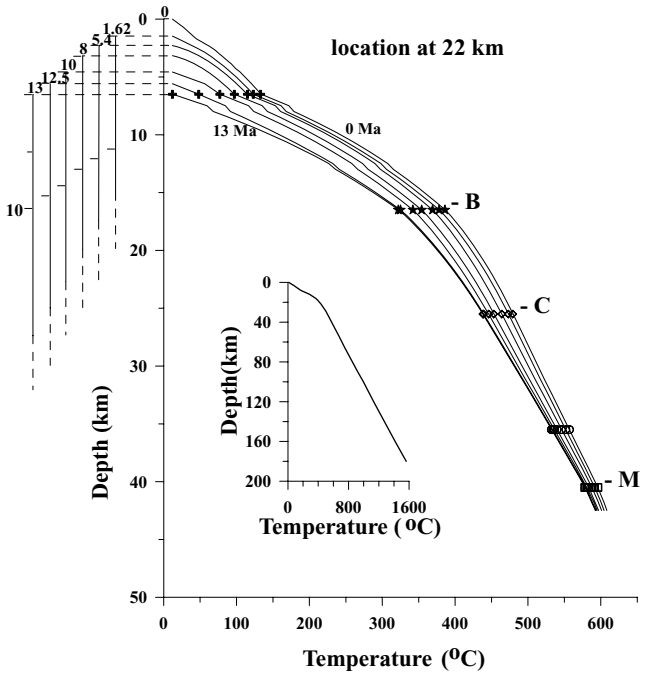


Figure 18. Temperature history of the rock volumes during Neogene–Quaternary sedimentation (13–0 Ma), for a location at 22 km on the study profile. B—crystalline basement, C—Conrad discontinuity, M—Mohorovičić discontinuity. Symbols—rock volumes. Note the different depth-axis corresponding to various time moments as marked. Inset: lithosphere-scale geotherm.

the different depth scales corresponding to various selected moments. The pressure–temperature–time paths of these rock volumes (not shown) suggest that metamorphic changes may have occurred as a consequence of sedimentation: Sarmatian rocks encountered Zeolite facies p – T conditions, Triassic rocks – Greenshists facies conditions, the upper crustal rocks – Amphibolite facies conditions and the lower crustal rocks – glaucofane-jadeite pressure – temperature conditions. Presently, the lithosphere is far from the estimated steady-state thermal conditions. The areas with the highest rate of sedimentation are the furthest from thermal equilibrium.

The thermal thickness of the lithosphere, as defined by the 0.85 Tm (Chapman *et al.* 1979), with Tm the melting temperature of mantle rocks at the corresponding depth, is in the study area about 160 km (see inset, Fig. 18 – the geotherm at lithospheric scale), about 20 km less than the first-order 1-D calculations of Demetrescu *et al.* (1984). It is also time dependent and will diminish to about 130–140 km at thermal equilibrium.

5.2.1 Sensitivity of temperature structure to model parameter changes

This issue has been discussed in several papers dealing with crustal geothermal modelling (e.g. Demetrescu 1982; Balling 1995). A detailed analysis can be found in Balling (1995).

In the present study, model uncertainty has been diminished in the first place by using mK range accurately measured temperatures in the depth range 70–2400 m as a reference, instead of the usual reference – the surface heat flux, which is a derived parameter. In our approach, the thermal conductivity in the mentioned depth range – the second parameter, which defines the surface heat flux besides the geothermal gradient –, becomes one of the model outputs and the

© 2007 The Authors, *GJI*, **170,** 896–912
Journal compilation © 2007 RAS

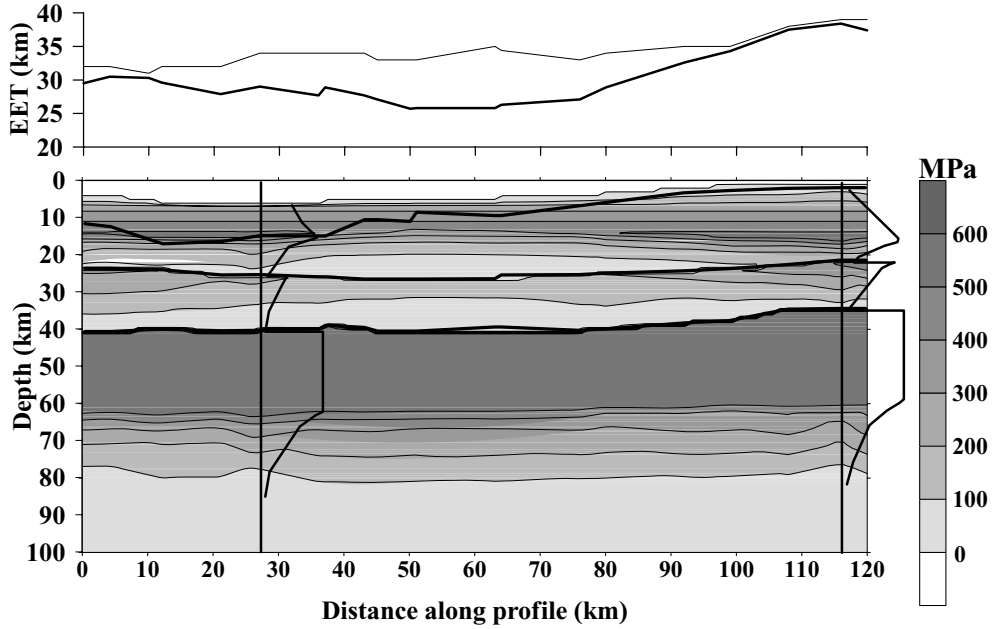


Figure 19. Rheological structure of the lithosphere (lower panel) and the corresponding effective elastic thickness (upper panel, thick line—Present, thin line—Pre-Sarmatian).

adopted structure and composition of sediments become key factors in modelling the thermal conductivity and further the crustal temperature field. We constrained these parameters by using best available information on the geological structure and sedimentation history. The composition of rocks has been detailed by using geophysical logging data. Also, the modelling took into account several aspects connected to the sedimentation process, such as the compaction of sediments and the polyphase nature of sedimentary rocks. Mean values from literature have been used for the thermal properties of constituents of sedimentary rocks. For the most part of the cross-section, sediment thermal conductivities have been altered during the trial-and-error process by amounts between -0.3 and 0.2 $W^{-1}m^{-1}K^{-1}$, with the exception of undercompacted shale volumes which required a reduction by as much as 0.8 $Wm^{-1}K^{-1}$. The fit to measured temperatures was improved from an overall standard deviation of $\pm 4.7\,^{\circ}$ to $\pm 0.46\,^{\circ}$C in this process. However, the consequences on the derived deeper temperature field are not significant, having in view the small thickness of various sedimentary layers involved (59 formations, 30–100 m thick).

5.3 On the rheological behaviour of the lithosphere in the study area

In the lower panel of Fig. 19, we plotted the present lithospheric rheological structure, corresponding to the temperature field illustrated in Fig. 17. It is based on 1-D vertical profiles (two of them are superimposed) calculated according to principles described by Ranalli & Murphy 1987; Ranalli 1995; Afonso & Ranalli 2004, for points along the study profile. Compressional strain and dry rheology have been used for crust and mantle rocks in the two equations describing the brittle (Sibson 1974), and respectively, the ductile (Kirby 1983) rheological regimes, namely:

$$\sigma_1 - \sigma_3 = \alpha \rho g z (1 - \lambda), \tag{3}$$

$$\sigma_1 - \sigma_3 = \left(\frac{\dot{\varepsilon}}{A}\right)^{\frac{1}{n}} \exp\left(\frac{E + PV}{nRT}\right), \tag{4}$$

Table 4. Parameters for rheological modelling* (Ranalli 1991).

	ρ (kg m^{-3})	E (kJmol^{-1})	n	A (Pa^{-n} s^{-1})
Upper crust	2700	230	3.0	$1.0 \cdot 10^{-21}$
Lower crust	2900	270	3.2	$1.99 \cdot 10^{-22}$
Mantle	3300	535	3.5	$3.16 \cdot 10^{-17}$

* $\dot{\varepsilon} = 2 \cdot 10^{14}$ s^{-1}; $\alpha = 3$; $\lambda = 0.36$.

where $\sigma_1 - \sigma_3$ is the maximum stress difference, α is a numerical factor depending on friction coefficient and fault type, ρ is the average density of rocks above the depth z, λ the pore fluid factor (ratio of pore fluid pressure to lithostatic pressure), $\dot{\varepsilon}$ the steady-state strain rate, T the absolute temperature, P the pressure, R the universal gas constant, E the creep activation energy, V the activation volume and n and A the material creep parameters. The actual values used in calculation are given in Table 4 (Ranalli 1995; Andreescu & Demetrescu 2001; Afonso & Ranalli 2004). Following Bassi (1995) we limited the strength at the maximum value of 600 MPa.

The interplay of composition and temperature controlled rheological properties of crust and mantle materials generally leads to a layered rheological model of lithosphere, with strong upper crust and subcrustal mantle separated by a ductile lower crust (Ranalli & Murphy 1987; Ranalli 1995). Recently, a discussion has been opened (Afonso & Ranalli 2004) on the validity of this model in comparison to a model of a strong 'seismic' crust overlying a weaker mantle. In our case, a study by Răileanu (1996) of the crustal rheology in the Focşani Basin seems to favour the sandwich model. The study showed that several sequences of earthquakes that have occurred in the area (R.Sărat) in the last three decades of the 20th century had a frequency-depth distribution of earthquakes very well correlated with the layered crustal rheological structure: the frequency of earthquake occurrence peaks in the depth ranges 17–20 and 28–34 km. These are precisely the stronger volumes of the upper crust and

lower crust, respectively, at the corresponding location (25–30 km from the beginning of the profile).

A direct consequence of the time-dependency of the lithosphere temperature field as a result of the sedimentation in the last 13 Myr is the alteration of the rheological properties of the lithosphere as compared to the pre-Sarmatian (>13 Myr) ones, both in the upper and in the lower crust, illustrated by the well-developed ductile layers ($\sigma_1 - \sigma_3 < 100$ MPa), which appear in the central part of the cross-section. The rheological structure before the sedimentation episode considered in this paper could be represented by the extreme left- and right-hand sides of the rheological cross-section, less affected by the recent sedimentation. Due to the lateral migration of the transient thermal anomaly induced by the deposition of Sarmatian sediments, at present its maximum and the corresponding maximum increase in upper and lower crust ductilities are to be found in the central part of the cross-section. The reduced mechanical strength of the lithosphere in the central part of the profile as compared to the pre-Sarmatian one is illustrated in the upper panel of Fig. 19, where the effective elastic thickness (EET) is plotted. Whereas, before 13 Ma EET varied laterally between 31 (western end of the profile) and 39 km (southeastern end), at present a diminished EET of ∼26–28 km characterizes a large segment of the profile. In the compressional environment in which the study area evolved in the last 13 Myr, a gradual propagation to the margin of the basin of the thermal anomaly induced in the underlying crust by the deposition of Sarmatian sediments, mimicked by a similar propagation of a diminished EET and of an increased capacity of the lithosphere to deform under lateral stress might be one of the reasons for the depocenter displacement and basin expansion noticed in the study area (Tărăpoancă *et al.* 2003). In comparison with our EET estimations, values of 10 and 15 km required by flexural modelling of the Focşani Basin, formation on top of the Moesian Platform (Tărăpoancă *et al.* 2004 and, respectively, Leever *et al.* 2006) are much too low. The values we obtained by geothermal and rheological modelling are in the range expected for a platform (Cloething & Burov 1996; Lankreijer *et al.* 1997; Andreescu & Demetrescu 2001).

6 CONCLUSIONS

The foreland of the Eastern Carpathians bend is a complex tectonic environment in the immediate vicinity of the well-known intermediate-depth seismogenic Vrancea zone. It includes the deepest sedimentary basin in Romania (∼18 km, eight of which being deposited in the last 13 Myr). The heat flux budget in the area plays a decisive role in defining the lithospheric rheological properties and their time evolution, of importance in geodynamic modelling of the orogen-foreland system, as well as in defining hydrocarbon generation conditions, of importance in oil and gas exploration and exploitation.

Detailed high-resolution temperature logs in the depth ranges from 0–700 m to 0–2400 m in eight thermally stabilized boreholes along a 120 km long profile in the foreland of the Eastern Carpathians bend have been used, together with logging and geological information on structure and lithology of the sedimentary pile to derive the time-dependent heat budget and temperature evolution of the lithosphere by means of a 2-D finite element model which includes sedimentation history, sediment compaction, lateral and vertical variation of thermal properties of sediments and consolidated crust. Modelling results have been compared to measured temperatures, corrected for palaeoclimate effects, in a trial-and-error iterative approach. A very good fit, within ±1 K has been obtained.

Sedimentation, palaeoclimate, undercompaction and heat refraction effects, on one hand, and the heat generated in the upper crust, on the other, combine to explain the observed subsurface temperature field, and in particular the pronounced curvature of the vertical temperature profiles.

Due to the interplay of thermal effects of high sedimentation rate episodes (13–12.5 Ma) and subsequent thermal relaxation and new sedimentation episodes, the overall effect of the Neogene–Quaternary sedimentation is rather uniform along the study profile – a deficit of about 12 mW m^{-2}, in spite of the large lateral variation of the sedimentary pile thickness. This is contrary to the common belief that the surface heat flux distribution in this basin is shaped by the sedimentary pile thickness. The strongest depression of the surface heat flux, of about 23 mW m^{-2}, occurred during the Sarmatian sedimentation (13–11 Ma) in the deepest part of the Focşani Depression on our profile (6 km in the last 13 Ma). It gradually recovered to the present day value.

The palaeoclimate effect is responsible for most of the observed curvature of the vertical temperature profiles and for a surface heat flux depression of 7–8 mW m^{-2}, uniform along the study profile. In young sedimentary basins such as the present case, both the thermal effects of rapid sedimentation and palaeoclimatic effects contribute to the temperature field in the upper part of the sedimentary section. With the depth of boreholes available, the two effects cannot be separated and inversion for palaeoclimate from measured borehole temperatures is not possible.

The lateral variation of the palaeoclimatically corrected surface heat flux from the centre of the Focşani Depression (40 mW m^{-2}) to its margin and the foreland platform (70 mW m^{-2}) is mainly the result of the lateral variation of the heat produced in the upper crust, from ∼15 mW m^{-2} in the deepest part of the depression (7 km of upper crust), to ∼36 mW m^{-2} in the central part of the depression (17 km of upper crust) and to about 45 mW m^{-2} in the platform area (21 km of upper crust). A heat production of 2.3 μW m^{-3} for the southeastern end of the profile and of 2.15 μW m^{-3} for the rest of it has been modelled.

The sedimentation process induces a significant time-dependency of the temperature field of the underlying lithosphere with repercussions on its thermal thickness, metamorphic state and rheological behaviour. Temperature variations as large as 70–100°C occurred in the crystalline crust immediately under the sedimentary pile. Progressively smaller variations were present up to 40–50 km depth. As a direct consequence of the temperature increase in the upper crust caused by sedimentation, the upper and the lower crust in the central part of the foreland basin at the present have a higher degree of ductility in comparison with the corresponding crustal volumes in the southeastern end of the study profile (EET values are 26–28 and 39 km, respectively). This has consequences for the mechanical interactions between the foreland and the orogen that lead to the formation and evolution of the Focşani Basin.

The modelling results indicate a thermally defined lithosphere thickness of about 160 km. The lithosphere has not reached yet the thermal steady – state, the present temperatures being about 80–90% of the equilibrium temperatures, depending on depth and on location along the study profile.

ACKNOWLEDGEMENTS

Part of the temperature data were obtained within the frame of the former Subproject A4 of the Sonderforschungsbereich 461

of Karlsruhe University. This study is supported by the Deutsche Forschungsgemeinschaft, project WI 687/15-1, and by the projects IG-02/2002–2004 of the Institute of Geodynamics, Bucharest. Financial support for presenting the paper at the International Meeting "New and classical applications of heat flow studies", Aachen, Germany, October 2004, was granted to CD by the project WI 687/15-1 and by the Organizing Committee of the meeting. The Romanian National Agency of Mineral Resources and PETROM S.A. are thanked for providing access to the wells and logging information. The detailed reviews by H. Schmeling and by an anonymous reviewer helped improving the submitted manuscript.

REFERENCES

Afonso, J.C. & Ranalli, G., 2004. Crust and mantle strengths in continental lithosphere: is the jelly sandwich model obsolete?, *Tectonophysics,* **394,** 221–232.

Akin, J.E., 1984. *Application and Implementation of Finite Element Methods*, Academic Press, London.

Andreescu, M., 1993. The inverse approach to a geothermal profile of the central Moesian Platform, Romania, *Tectonophysics,* **224,** 435–442.

Andreescu, M. & Demetrescu, C., 2001. Rheological implications of the thermal structure of the lithosphere in the convergence zone of the Eastern Carpathians, *J. Geodynamics,* **31,** 373–391.

Andreescu, M., Nielsen, S.B., Polonic, G. & Demetrescu, C., 2002. Thermal budget of the Transylvanian lithosphere. Reasons for a low surface heat-flux anomaly in a Neogene intra-Carpathian basin, *Geophys. J. Int.,* **150,** 494–505.

Balling, N., 1995. Heat flow and thermal structure of the lithosphere across the Baltic Shield and northern Tornquist Zone, *Tectonophysics,* **244,** 13–50.

Bassi, G., 1995. Relative importance of strain rate and rheology for the mode of continental extension, *Geophys. J. Int.,* **122,** 195–210.

Bădescu, D., 1998. Geology of the Eastern Carpathians – an overview, in *Monograph of Southern Carpathians*, pp. 49–70, ed. Sledzinski, I., Politechnika Warszawska, *Reports on Geodesy*, **7**, Warszaw.

Beck, A.E., 1976. An improved method of computing the thermal conductivity of fluid filled sedimentary rocks, *Geophysics,* **41,** 133–144.

Beck, A.E., 1977. Climatically perturbed temperature gradients and their effect on regional and continental heat flow means, *Tectonophysics,* **41,** 17–39.

Beck, A.E. & Shen, P.Y., 1989. On a more rigorous approach to geothermic problems, *Tectonophysics,* **164,** 83–92.

Blackwell, D.D. & Steele, J.L., 1986. Thermal conductivity of sedimentary rocks: Measurement and significance, in *Thermal History of Sedimentary Basins*, pp. 13–37, eds. Naeser, N.D. & McCulloh, T.H., Springer-Verlag, New York, Berlin, Heidelberg.

Carlsaw, H.S. & Jaeger, J.C., 1959. *Conduction of Heat in Solids*, Oxford Univ. Press, Oxford, 510 pp.

Čermák, V., 1995. A geothermal model of the central segment of the European Geotraverse, *Tectonophysics,* **244,** 51–55.

Čermák, V. & Bodri, L., 1991. A heat production model of the crust and upper lithosphere, *Tectonophysics,* **194,** 304–323.

Čermák, V., Šafanda, J. & Guterch, A., 1989. Deep temperature distribution along three profiles crossing the Teisseyre-Tornquist tectonic zone in Poland, *Tectonophysics,* **164,** 151–163.

Chapman, D.S., Pollack, H.N. & Čermák, V., 1979. Global heat flow with special reference to the region of Europe, in *Terrestrial Heat Flow in Europe*, pp. 41–48, eds. Čermák, V. & Rybach, L., Springer, Berlin, Heidelberg, New York.

Clauser, C. *et al.* 1997. The thermal regime of the crystalline continental crust – implications from the KTB, *J. Geophys. Res.,* **102,** 18417–18441.

Cloething, S. & Burov. E.B., 1996. Thermomechanical structure of European continental lithosphere: constraints from rheological profiles and EET estimates. *Geophys. J. Int.,* **124,** 695–723.

Damian, A., 1996. Hydrocarbon in overpressured pelitic Neogene bodies from the Focşani Depression, Romania, in *Oil and Gas in Alpidic Thrustbelts and Basins of Central and Eastern Europe*, pp. 309–314, eds. G. Wessely & Liebl, W., EAGE Special Publication No. 5, Amsterdam.

Demetrescu, C., 1982. Thermal structure of the crust and upper mantle in Romania, *Tectonophysics,* **90,** 123–135.

Demetrescu, C. & Andreescu, M., 1994. On the thermal regime of some tectonic units in a continental collision environment in Romania, *Tectonophysics,* **230,** 265–271.

Demetrescu, C. & Polonic, G., 1989. The evolution of the Pannonian Depression (Romanian sector) as derived from subsidence and heat flow data, *Tectonophysics,* **164,** 287–299.

Demetrescu, C., Ene, M. & Andreescu, M., 1981. On the geothermal regime of Transylvanian Depression, *St. cer. Geol., Geofiz., Geogr., Ser. Geofiz.,* **19,** 61–71.

Demetrescu, C, Andreescu, M. & Ene, M., 1984. On the thermal structure of the lithosphere in Romania, *Rev. Roum. Géol., Géophys., Géogr., Ser, Géophys.,* **28,** 19–33.

Demetrescu, C., Veliciu, S. & Burst, A.D., 1991/1992. Heat flow map of Romania, in *Geothermal Atlas of Europe*, pp. 72–74, eds. Hurtig, E., Čermák, V., Haenel, R. & Zui, V., VEB Herrmann Haack, Gotha, Leipzig.

Demetrescu, C., Nielsen, S.B., Ene, M., Şerban, D.Z., Polonic, G., Andreescu, M., Pop, A. & Balling, N., 2001. Lithosphere thermal structure and evolution of the Transylvanian Depression – insights from new geothermal measurements and modelling results, *Phys. Earth Planet. Inter.,* **126,** 249–267.

Demetrescu, C., Wilhelm, H., Ene, M., Andreescu, M., Polonic, G., Baumann, C., Dobrică, V. & Şerban, D.Z., 2005. On the geothermal regime of the foreland of the Eastern Carpathians bend. *J. Geodyn.,* **39,** 29–59.

Demezhko, D. & Shchapov, V., 2001. 80 000 years ground surface temperature history inferred from the temperature – depth log measured in the superdeep hole SG – 4 (the Urals, Russia), *Glob Planet. Change,* **29,** 219–230.

Demezhko, D., Outkin, V., Duchov, A., Balobaev, V. & Ryvkin, D., 2006. Spatial distribution of Pleistocene/Holocene warming amplitudes in northern Eurasia inferred from geothermal data, Abstract, *Sixth International Meeting "Heat Flow and the Structure of the Lithosphere"*, Bykov, Czech Republic, June 5–10, 2006.

Demongodin, L., Pinoteau, B., Vasseur, G. & Gable, R., 1991. Thermal conductivity and well logs: a case study in the Paris Basin, *Geophys. J. Int.,* **105,** 675–691.

Dumitrescu, I. & Săndulescu, M., 1970. Tectonic map of Romania, scale 1:1.000.000, *Geological Atlas, Sheet no.6*, Geologic Institute, Bucharest.

Ene, M., Andreescu, M. & Demetrescu, C., 1989–1990. *Annual Internal Reports*, Institute of Geodynamics, Bucharest.

Enescu, D., 1992. Lithosphere structure in Romania. I. Lithosphere thickness and average velocities of seismic waves P and S. Comparison with other geophysical data, *Rev. Roum. Phys.,* **37,** 623, 639.

Hauser, F., Raileanu, V., Fielitz, W., Bala, A., Prodehl, C, Polonic, G. & Schulze, A, 2001. VRANCEA99 – the crustal structure beneath the southeastern Carpathians and the Moesian Platform from a seismic refraction profile in Romania, *Tectonophysics,* **340,** 233–256.

Holbrook, S., Mooney, W.D. & Christensen, N.I., 1992. The seismic velocity structure of the deep continental crust, in *Continental Crust*, eds. D.M. Fountain, R. Arculus, R. Kay, Elsevier, New York, 1–43.

Hutchison, I., 1985. The effect of sedimentation and compaction on oceanic heat flow, *Geophys. J. R. Astr. Soc.,* **82,** 439–459.

Issler, D.R. & Beaumont, C., 1986. Finite element model of the subsidence and thermal evolution of extensional basins: Application to the Labrador Continental Margin, in *Thermal History of Sedimentary Basins*, pp. 239–268, eds. Naeser, N.D. & McCulloh, T.H., Springer-Verlag, New York, Berlin, Heidelberg.

Kappelmeyer, O. & Haenel, R., 1974. *Geothermics with Special Reference to Application*, Gebrüder Borntraeger, Berlin.

Kirby, S.H., 1983. Rheology of the lithosphere, *Rev. Geophys. Space Phys.,* **21,** 1458–1487.

© 2007 The Authors, *GJI*, **170,** 896–912
Journal compilation © 2007 RAS

Lankreijer, A., Mocanu, V. & Cloething, S., 1997. Lateral variations in lithosphere strength in Romanian Carpathians: constraints on basin evolution, *Tectonophysics,* **272,** 269–290.

Leever, K.A., Bertotti, G., Zoetemeijer, R., Matenco, L. & Cloething, S., 2006. The effect of a lateral variation in lithospheric strength on foredeep evolution: Implications for the East Carpathians foredeep, *Tectonophysics,* **421,** 251–267.

Magara, K., 1986. Porosity-depth relationship during compaction in hydrostatic and non-hydrostatic cases, in *Thermal Modelling in Sedimentary Basins*, pp. 129–149, ed. Burrus, J., Editions Technip, Paris.

Mareschal, J.C., Rolandone, F., Bienfait, G., 1999. Heat flow variations in a deep borehole near Sept-Iles, Quebec, Canada: Paleoclimatic interpretation and implications for regional heat flow estimates, *Geophys. Res. Lett.,* **26,** 2049–2052.

McKenzie, D.P., 1978. Some remarks on the development of sedimentary basins, *Earth Planet. Sci. Lett.,* **40,** 25–32.

Paraschiv, D., 1979. *The Moesian Platform and its Hydrocarbon Deposits*, pp. 195, Romanian Academy Press, Bucharest.

Pasquale, V., Verdoya, M. & Chiozzi, P., 2001. Radioactive heat generation and its thermal effects in the Alps-Apennines boundary zone, *Tectonophysics,* **331,** 269–283.

Polonic, G., 1996. Structure of the crystalline basement in Romania, *Rev. Roum. Géophys.,* **40,** 57–69.

Ranalli, G., 1991. Regional variations in lithospheric rheology from heat flow observations, in *Terrestrial Heat Flow and the Lithosphere Structure*, pp. 1–22, eds. V. Čermák & L. Rybach, Springer-Verlag, Berlin, Heidelberg, New York.

Ranalli, G., 1995. *Rheology of the Earth*, 2nd edn., Chapman and Hall, New York.

Ranalli, G. & Murphy, D.C., 1987. Rheological stratification of the lithosphere, *Tectonophysics,* **132,** 281–295.

Rădulescu, F., 1988. Seismic models of the crustal structure in Romania, *Rev. Roum., Géol., Géophys., Géogr., Ser. Géophys.,* **32,** 13–17.

Rădulescu, F., Demetrescu, C., Biter, M., Andreescu, M., Răileanu, V. & Ene, M., 1985. Lithospheric structure along the Galaţi-Chişineu Criş and Iaşi-Turnu Măgurele profiles, *Rev. Roum. Phys.,* **30,** 151–160.

Răileanu, V., 1996. Rheology of the crust for Râmnicu Sărat area, *Rev. Roum. Géophys.,* **40,** 33–44.

Răileanu, V., 1998. Study of Some Physical Parameters of Lithosphere in Selected Areas in Romania, *PhD thesis*, Institute of Atomic Physics, Bucharest.

Romanian Geological Survey, 1968. *Geological Map of Romania, scale 1: 200,000*, Bucharest.

Rybach, L., 1988. Determination of heat production rate, in *Handbook of Terrestrial Heat Flow Density Determination*, pp. 125–142, eds. Haenel, R., Rybach, L. & Stegena, L., Kluwer Academic Publishers, Dordrecht.

Šafanda, J. & Rajver, D., 2001. Signature of the last ice age in the present subsurface temperatures in the Czech Republic and Slovenia, *Glob Planet. Change,* **29,** 241–257.

Sanders, C., Andriessen, P. & Cloetingh, S., 1999. Life cycle of the East Carpathian Orogen: erosion history of a doubly vergent critical wedge assessed by fission track thermochronology, *J. Geophys. Res.,* **104,** 29,095–29,112.

Săndulescu, M., 1984. *Geotectonics of Romania*, pp.334, Technical Press, Bucharest.

Schön, J.H., 1996. Physical Properties of Rocks: Fundamentals and Principles of Petrophysics, in *Handbook of Geophysical Exploration: Seismic Exploration*, **18**, Elsevier, Amsterdam.

Sclater, J.G. & Christie, P.A.F., 1980. Continental stretching and explanation of the post-mid-cretaceous subsidence of the Central North Sea Basin, *J. Geophys. Res.,* **85,** 3711–3749.

Sibson, R.H., 1974. Frictional constraints on thrust, wrench and normal faults, *Nature,* **249,** 542–544.

Steckler, M.S. & Watts, A.B., 1978. Subsidence of the Atlantic type continental margin off New York, *Earth Planet. Sci. Lett.,* **41,** 1–13.

Stănică, D. & Stănică, M., 1984. Crust and upper mantle investigation by magnetotelluric soundings in Romania, *Acta Geodetica, Geophysica et Montanistica Hungariae,* **19,** 147–152.

Şerban, D.Z., Nielsen, S.B. & Demetrescu, C., 2001a. Transylvanian heat flow in the presence of topography, paleoclimate and groundwater flow, *Tectonophysics,* **335,** 331–344.

Şerban, D.Z., Nielsen, S.B. & Demetrescu, C., 2001b. Long wavelength ground surface temperature history from continuous temperature logs in the Transylvanian Basin, *Glob Planet. Change,* **29,** 201–217.

Tarantola, A. & Valette, B., 1982a. Inverse problems – quest for information, *J. Geophys.,* **50,** 159–170.

Tarantola, A. & Valette, B., 1982b. Generalized nonlinear inverse problems solved using the least squares criterion, *Rev. Geophys. Space Phys.,* **20,** 219–232.

Tărăpoancă, M., Bertotti, G., Maţenco, L., Dinu, C. & Cloetingh, S.A.P.L., 2003. Architecture of the Focşani Depression: A 13 km deep basin in the Carpathians bend zone (Romania), *Tectonics,* **22,** 1074, doi:10.1029/2002/TC001486.

Tărăpoancă, M., Garcia-Castellanos, D., Bertotti, G., Matenco, L., Cloething, S. & Dinu, C., 2004. Role of 3-D distributions of load and lithospheric strength in orogenic arcs: polystage subsidence in the Carpathians foredeep, *Earth Planet. Sci. Lett.,* **221,** 163–180.

Vasseur, G., Brigaud, F. & Demongodin, L., 1995. Thermal conductivity estimations in sedimentary basins, *Tectonophysics,* **244,** 167–174.

Zugrăvescu, D., Polonic, G., Horomnea, M. & Dragomir, V., 1998. Recent vertical movements on the Romanian territory, major tectonic compartments and their relative dynamics, *Rev. Roum. Géophysique,* **42,** 3–14.

APPENDIX A: THERMAL MODELLING METHODOLOGY

This appendix describes how the processes of sedimentation and erosion are represented in the thermal finite element model.

The process of compaction and lithology variations prompt the use of a Lagrangian finite element grid to represent the sediments, that is the nodes of the grid follow fixed sedimentary particles. At the surface, however, sedimentary material must cross the boundary of the finite element grid in the case of erosion or sedimentation.

Model evolution starts with calculation of the steady-state thermal solution for the initial model configuration, that is typically a part of the upper mantle, crystalline crust, perhaps some initial

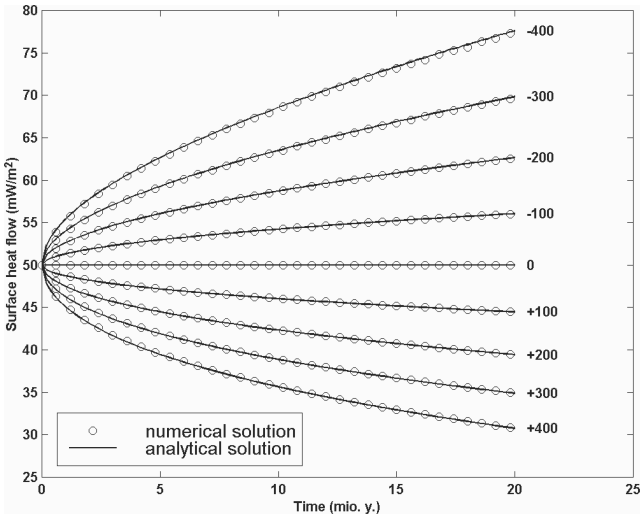


Figure A1. Surface heat flow as a function of time for constant erosion or sedimentation. Curve parameter is meters of erosion or sedimentation per million years. The analytical solution is from Carslaw and Jaeger (1959). The thermal diffusivity is 8.333e−007 m^2/s and the sub time step $\Delta t =$ 0.2 Ma. $\Delta t = 0.5$ Ma produces no recognisable difference.

© 2007 The Authors, *GJI*, **170,** 896–912
Journal compilation © 2007 RAS

sediment and the appropriate boundary conditions. The sedimentation and erosion history that follows is divided into master events corresponding to the geological periods of typical duration some millions of years, each of which is further subdivided into a number of short-duration sub time steps ($\Delta t = 0.1$ to 0.5 Ma) of either sedimentation or erosion. The sedimentation/erosion history is specified a priori at a number of locations along the profile, between which there is linear interpolation of the thickness added or removed during each event. At the onset of a new event of sedimentation, a new row of elements is activated and the thickness of the top row of elements is adjusted to accommodate the thickness of sediments added during sub time step Δt. As a consequence of adding sediments at the surface, the sedimentary layers below (and the sediments of the top layer) are being buried at a greater depth wherefore they are compacted according to the exponential compaction law and the compaction parameters (Φ_0 and L) that are valid for the particular lithology of each layer. After adding sediments, the system matrix is assembled with the new conductivity and heat production structure, the boundary conditions appropriate to the age in question (surface temperature and background heat flux) are applied and the solution is propagated forward in time by the time step Δt. We use fully implicit time integration. In the event of a very high rate of sedimentation during a master event, several rows of elements are being created in order to represent the transient thermal solution more accurately. Experience shows that a typical maximum element height of about 50 m is suitable. Thinner sedimentary layers will of course be represented by the appropriate element thickness. The thermal finite element code is very stable and elements thickness down to 1 m pose no problem. Erosion episodes are represented as sedimentation events which are to be removed later. During removal of the number of finite element layers that represent the event to be removed, the above procedure is carried out in reverse order, except that there is no decompaction. It is the maximum depth of burial that determines the degree of compaction of a sedimentary layer. The transient thermal effects of even very high rates of erosion and sedimentation are well represented by this procedure (Figure A1).

© 2007 The Authors, *GJI*, **170,** 896–912
Journal compilation © 2007 RAS